Cell Reports

Article

CD4 CTLs in supercentenarians: Signs of adaptive expansion in healthy aging

Graphical abstract

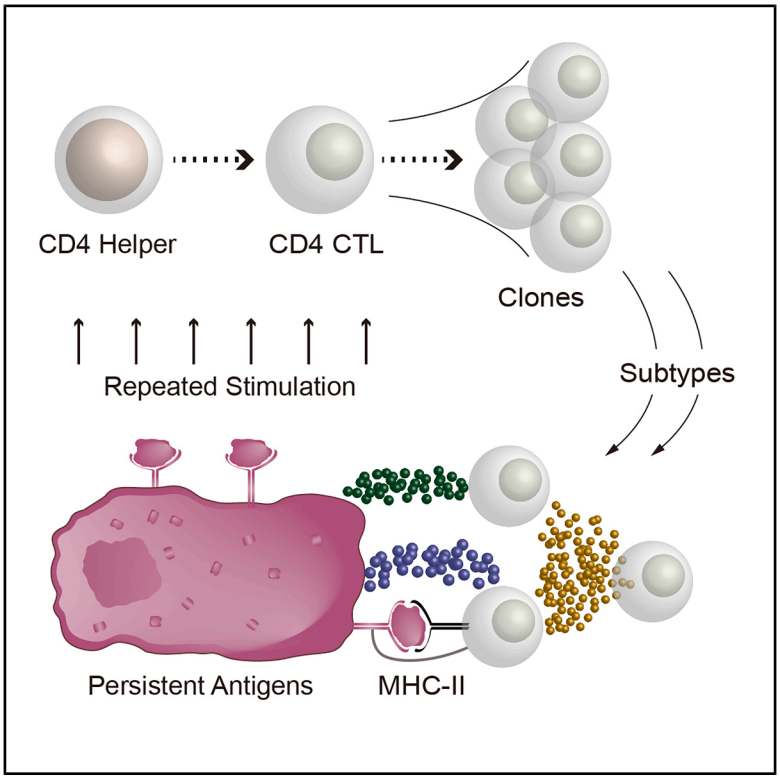

Authors

Kosuke Hashimoto, Miki Kojima-Ishiyama, Hajime Inokuchi, ..., Nobuyoshi Hirose, Piero Carninci, Yasumichi Arai

Correspondence

kosuke.hashimoto@protein.osaka-u.ac.jp (K.H.), nakano.ggbb@gmail.com (N.H.), carninci@riken.jp (P.C.), yasumich@keio.jp (Y.A.)

In brief

Hashimoto et al. show that CD4 CTLs expand around age 100 and form large private clones without exhaustion. These cells exhibit stepwise differentiation and cytokine plasticity, suggesting adaptive responses to persistent antigens during healthy aging.

Highlights

- CD4 CTLs expand around age 100 without signs of exhaustion
- A $CD27^{-}CD28^{+}$ state marks the intermediate helper-to-killer transition
- Large private CD4 CTL clones suggest repeated antigen exposure
- Single clones diversify cytokine profiles after *ex vivo* stimulation

Hashimoto et al., 2026, Cell Reports ■■, 117728
■■, 2026
https://doi.org/10.1016/j.celrep.2026.117728

CellPress

Please cite this article in press as: Hashimoto et al., CD4 CTLs in supercentenarians: Signs of adaptive expansion in healthy aging, Cell Reports (2026), https://doi.org/10.1016/j.celrep.2026.117728

Cell Reports

CellPress
OPEN ACCESS

Article

CD4 CTLs in supercentenarians: Signs of adaptive expansion in healthy aging

Kosuke Hashimoto,[1,2,6,*] Miki Kojima-Ishiyama,[2] Hajime Inokuchi,[2,3] Michihira Tagami,[2] Takashi Sasaki,[4] Kenji Mizuguchi,[1] Yasushi Okazaki,[2] Ichiro Taniuchi,[2] Kazuyoshi Ishigaki,[2,3] Nobuyoshi Hirose,[4,*] Piero Carninci,[2,5,*] and Yasumichi Arai[4,*]

[1]Institute for Protein Research, The University of Osaka, Osaka 565-0871, Japan
[2]RIKEN Center for Integrative Medical Sciences, Yokohama 230-0045, Japan
[3]Department of Microbiology and Immunology, Keio University School of Medicine, Tokyo 160-0016, Japan
[4]Centre for Supercentenarian Medical Research, Keio University School of Medicine, Tokyo 160-0016, Japan
[5]Human Technopole, via Rita Levi Montalcini 1, Milan, Italy
[6]Lead contact
*Correspondence: kosuke.hashimoto@protein.osaka-u.ac.jp (K.H.), nakano.ggbb@gmail.com (N.H.), carninci@riken.jp (P.C.), yasumich@keio.jp (Y.A.)
https://doi.org/10.1016/j.celrep.2026.117728

SUMMARY

Our previous study identified CD4 cytotoxic T lymphocytes (CD4 CTLs) as a hallmark of supercentenarians. CD4 CTLs have primarily been studied in disease contexts; however, their role in healthy aging remains unclear. Using single-cell immune profiling, we analyzed T cells from supercentenarians and found that CD4 CTLs begin to expand around the age of 100, characterized by sequential CD27/CD28 loss without exhaustion. CD4 CTLs were dominated by large clones, with top clones averaging 33.3%, indicating repeated stimulation by persistent antigens. Furthermore, CDR3β sequences of the top clones matched those of T cells expanded in tumors, particularly lung cancer. *Ex vivo* stimulation experiments revealed that CD4 CTLs consist of subgroups defined by interleukin expression patterns, suggesting their plasticity within the same clone. These findings suggest that CD4 CTLs expand and diversify as an adaptation to persistent antigens, potentially contributing to longevity through cancer suppression.

INTRODUCTION

Aging is an inevitable biological process, characterized by gradual declines in physical and cognitive functions. This process is driven by the accumulation of molecular and cellular alterations, including DNA mutations, mitochondrial dysfunction, and cellular senescence.[1,2] Among these changes, the aging of the immune system compromises its ability to defend against external pathogens and eliminate internal abnormal cells such as precancerous or senescent cells, increasing the risk of various diseases.[3–5] However, aging itself is not a disease, nor does it necessarily lead to the failure of essential physiological systems. Supercentenarians—individuals who live to or beyond 110 years—provide a model of healthy aging, achieving longevity while avoiding or delaying major age-related diseases such as cardiovascular disorders and cancer. They maintain immune,[6] cardiovascular,[7] and epigenomic[8] profiles that appear younger than expected for their chronological age. Furthermore, our recent genetic study on Japanese centenarians, including 173 supercentenarians, identified key genetic components associated with longevity and their correlation with reduced risks of multiple age-related diseases,[9] suggesting a potential genetic contribution to sustained immune function in advanced age.

Our previous study revealed that supercentenarians possess a high frequency of CD4 cytotoxic T lymphocytes (CD4 CTLs) in their peripheral blood mononuclear cells (PBMCs).[10] These CD4 CTLs typically exhibited loss of CD27 and CD28, a characteristic commonly associated with highly differentiated CD4 and CD8 T cells in the context of aging.[11,12] Significant accumulation of CD4 CTLs has also been reported in 24-months-old mice.[13] CD4 CTLs are an unusual subset of T cells that express both CD4 and cytotoxic effector molecules, making them an exception to the conventional $CD4^{-}$and CD8-lineage classification. Under normal conditions, CD4 CTLs are rare in the peripheral blood, typically accounting for less than 5% of the total T cell population.[10,14] In contrast, CD4 CTLs have been consistently detected in the context of viral infections such as CMV, HIV, and SARS-CoV-2, where several studies have reported their antiviral activity through perforin/granzyme secretion and Fas/FasL-mediated pathways.[15–18] In addition, recent studies have demonstrated that CD4 CTLs exhibit the ability to kill tumor cells in an MHC class II-dependent manner across various cancer types, including non-small cell lung cancer (NSCLC),[19] bladder cancer,[20] melanoma,[21] and colorectal cancer.[22] However, the role of CD4 CTLs in the context of healthy aging remains unclear, particularly in individuals such as supercentenarians, who maintain a healthy state with high frequency of CD4 CTLs.

A recent study has provided new insights into CD4 CTL activity, demonstrating their ability to eliminate senescent fibroblasts in aging human skin through the recognition of viral antigens.[23]

Please cite this article in press as: Hashimoto et al., CD4 CTLs in supercentenarians: Signs of adaptive expansion in healthy aging, Cell Reports (2026), https://doi.org/10.1016/j.celrep.2026.117728

This suggests a potential role of CD4 CTLs in supporting anti-aging processes by targeting senescent cells. In this study, we investigated CD4 CTLs across different age groups, focusing on supercentenarians as a model of healthy aging, through an integrated analysis of their transcriptome, surface proteins, and TCR profiles. Our results revealed that CD4 CTLs expand with age and exhibit plasticity in cytokine production. This suggests that CD4 CTLs may contribute to cancer suppression and longevity through adaptive responses to persistent antigens, emphasizing their role in immune resilience and healthy aging.

RESULTS

Identification of CD4 CTLs in all age groups

We generated three types of single-cell profiles—transcriptome, surface protein, and TCR sequences—from T cells in blood from eight donors aged in their 70s–90s (group A), 10 centenarians (group B), and 10 supercentenarians (group C) (Figures 1A and S1A). After demultiplexing samples using hashtags (Figures S1B–S1D), we filtered out low-quality cells (Figures S1E–S1G; see STAR Methods for details). QC validation further confirmed data consistency across samples, including comparable gene and UMI counts (Figure S1H) and absence of sample-specific bias in UMAP space (Figure S1I). A total of 43,584 T cells (14,604 for group A; 14,599 for B; and 14,381 for C) were compiled for the primary analysis. The cells were classified into 13 clusters shown on UMAP (Figures 1B and S1J), with CD4 (4 clusters), CD8 (3 clusters), and γδ T cells as the major categories. Smaller clusters included MKI67$^+$ proliferating T cells, MAIT cells, γδ T cells, and remaining non-T-cell contaminants. Within the CD4 clusters, we identified CD4 CTLs by the co-expression of CD4 and cytotoxic genes such as *GZMB* and *GZMH*, alongside CD4 naive, CD4 helper, and Tregs.

We then compared the proportions of these CD4 clusters among three age groups and found a significant monotonic increase in CD4 CTLs with age (p = 0.029, Jonckheere-Terpstra test) (Figure 1C). The median percentages of CD4 CTLs were 4.0%, 9.6%, and 17.6% in groups A, B, and C, respectively. Notably, the expansion of CD4 CTLs is not specific to supercentenarians; one donor under the age of 100 exhibited the highest proportion of CD4 CTLs. This individual (A08) was clinically healthy and had no QC abnormalities. Similar to supercentenarians, A08 showed an increased proportion of CD4 CTLs, accompanied by relatively low levels of CD4 Naive and Helper cells. These findings suggest that CD4 CTL expansion can also occur in younger individuals without signs of pathology or quality issues.

To investigate the dynamics of CD4 CTL proportions across a broad age spectrum, we collected and integrated public single-cell datasets, encompassing over 5 million cells from 1,512 samples and covering an age range from 0 to over 110 years (Figure S1K).[10,24–28] Initial prediction attempts using existing tools, such as CellTypist,[29] resulted in the misclassification of CD4 CTLs as CD8 T cells (Figure S1L). To overcome this annotation challenge, we developed a multi-task VAE model trained on our primary dataset (Figure S1M). The predictive performance of this model was validated using an independent dataset (GSE164378),[30] achieving a robust F1 score of approximately 0.8 (Figures S1L and S1N). By applying this validated VAE to the integrated public datasets, we revealed that while the proportion of CD4 CTLs remains low in younger individuals, both the median and variance of this population increase markedly at extreme old age (Figure 1D).

Identification of an intermediate in helper-to-killer transition

We investigated the *trans*-differentiation process from CD4 helper to CTL using TotalSeq-C barcoded antibodies tagged with 16 distinct cell surface markers (marked as primary in Figure S2A), which allowed us to analyze surface proteins in single-cell RNA sequencing datasets. We found that CD4 CTLs are characterized by the loss of co-stimulation factors CD27 and CD28, which distinguishes them from the other three CD4 clusters (Figure 2A). A fraction of these CD4 CTLs exhibited mid-level CD8 expression (Figure 2A, lower right). This signal was clearly lower than the robust CD8 expression in canonical CD8 T cells (Figure S2B; detailed in a later section). Additionally, consistent with previous reports that CD4 CTLs show a highly differentiated CD27$^-$CD28$^-$CD45RO$^+$CD45RA$^-$CCR7$^-$ phenotype,[14,31,32] our CD4 CTLs displayed a distinctive marker profile of CD95^{mid}, CCR7$^-$, CD45RA$^-$, CD45RO$^+$, and PD-1$^-$ (Figure S2C), indicating their advanced differentiation without signs of exhaustion. This phenotype was further supported by transcriptional analysis, which confirmed the expression of CTL-associated surface markers, chemokines, and transcription factors,[33–36] along with low levels of exhaustion-related genes such as *TIGIT*, *CTLA4*, and *LAG3* (Figure S2D).

We identified a CD27$^-$CD28$^+$ population, as highlighted in circles in Figure 2A, as cells in a potential transient state from CD4 helper to CTL. This group constitutes 10.5% of the CD4 T cell population, in contrast to the CD27$^+$CD28$^-$ population of less than 0.3% (Figure 2B, left). The minimal presence of CD27$^+$CD28$^-$ cells implies a sequential order during this transition—initially the loss of CD27, followed by loss of CD28. Indeed, CD27$^-$CD28$^+$ cells are situated at the interface between helper and CTL clusters on the UMAP, serving as a connective bridge between the two cell types (Figure 2B, right).

We analyzed the transcriptome of the CD27$^-$CD28$^+$ population, initially identified through surface protein expression. Consistent with the protein profiles, RNA expression of CD27 was diminished in this population, whereas CD28 RNA was maintained at levels similar to those in helper T cells (Figure 2C). Notably, the expression levels of cytotoxic genes such as granzymes and perforin were intermediate between the helper and CTL clusters (Figures 2C and S2E). This pattern extended to transcription factors associated with CTLs such as *TBX21* and *EOMES*, reinforcing the transitional nature of CD27$^-$CD28$^+$ cells.

To validate these populations, we performed flow cytometry and bulk RNA sequencing on sorted cells. Flow cytometry confirmed the existence of both the CD27$^-$CD28$^-$ and the CD27$^-$CD28$^+$ populations within the CD3$^+$CD4$^+$ T cell compartment (Figure 2D). Furthermore, bulk RNA-seq of sorted subsets from one donor showed that the CD27$^-$CD28$^-$ T cells expressed higher levels of cytotoxic genes and related transcription factors compared to the CD45RO$^+$CD28$^+$ T cells (Figures 2E and S2F).

Please cite this article in press as: Hashimoto et al., CD4 CTLs in supercentenarians: Signs of adaptive expansion in healthy aging, Cell Reports (2026), https://doi.org/10.1016/j.celrep.2026.117728

CellPress
OPEN ACCESS

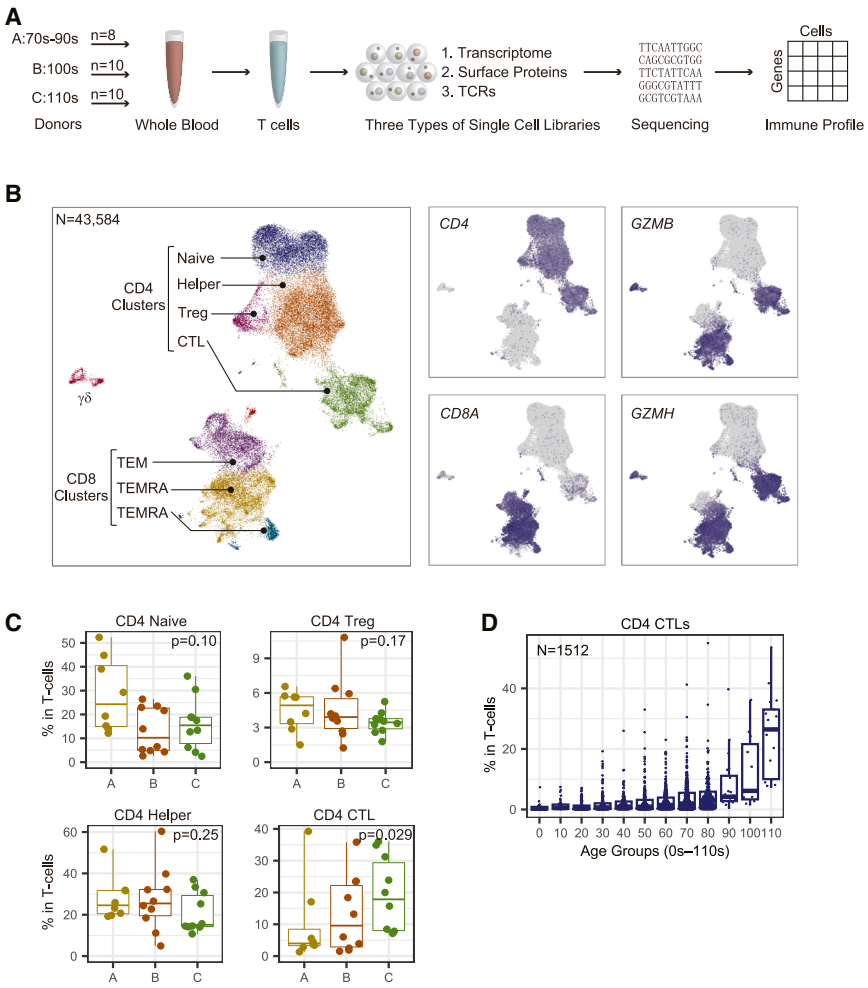

Figure 1. Overview of single-cell immune profiling

(A) Workflow for generating T cell profiles from donors 70s–90s (group A, *n* = 8), centenarians (group B, *n* = 10), and supercentenarians (group C, *n* = 10).

(B) UMAP projection based on both transcriptome and surface protein data. Seven major clusters, including CD4 CTL shown in green, are indicated in the left panel. Notably, the smaller of the two CD8 TEMRA clusters was predominantly composed of cells from donor B09, suggesting a donor-specific subpopulation. The right panels show RNA expression levels of *CD4*, *CD8A*, *GZMB*, and *GZMH*.

(C) Subset frequency comparison across age groups. Monotonic trends across age groups were assessed using the two-sided Jonckheere-Terpstra test. A significant increasing trend was observed for CD4 CTLs ($p = 0.029$).

(D) Dynamics of CD4 CTL proportions across a broad age spectrum (0s–110s). The boxplots show the percentage of CD4 CTLs among T cells across 1,512 integrated public samples, as predicted by the trained VAE model. Boxplots: center, median; hinges, 25th/75th percentiles; whiskers, 1.5 × IQR. Dots: each donor (C) or sample (D).

Non-canonical TCR features in CD4 CTLs: clonal expansion, dual TCR expression, and TCRγ gene activation

Following our characterization of differentiation in CD4 CTLs, we further investigated their TCR repertoire to gain insights into their clonal structure and receptor composition. We observed that CD4 CTLs were clonally expanded in all samples, including those from non-centenarians, as indicated by high Simpson's index values and low Shannon diversity (Figure S3A). Notably, the largest clone accounted for an average of 33.3% of the CD4 CTLs (Figure 3A). For example, in centenarian sample B04, the largest clone comprised 126 of the 234 CD4 CTL cells, representing 53.8% of the population (Figure S3B). This finding indicates that clonal expansion, producing a few dominant clones, is one of the driving forces behind the increase in CD4 CTLs. However, as comparable expansion was observed across all age groups, it alone does not explain the higher frequencies in supercentenarians, suggesting that additional factors, such as the duration of antigenic stimulation, influence the scale of expansion.

We compared the CDR3α and CDR3β sequences of the largest clones across 28 individuals. All individuals had unique sequences, with no public TCRs identified (Figures 3B and S3C). Interestingly, five top clones of 28 exhibited dual TCR expression—two distinct alpha chains or two distinct beta chains expressed in a single T cell (Figure 3B). To validate the

Please cite this article in press as: Hashimoto et al., CD4 CTLs in supercentenarians: Signs of adaptive expansion in healthy aging, Cell Reports (2026), https://doi.org/10.1016/j.celrep.2026.117728

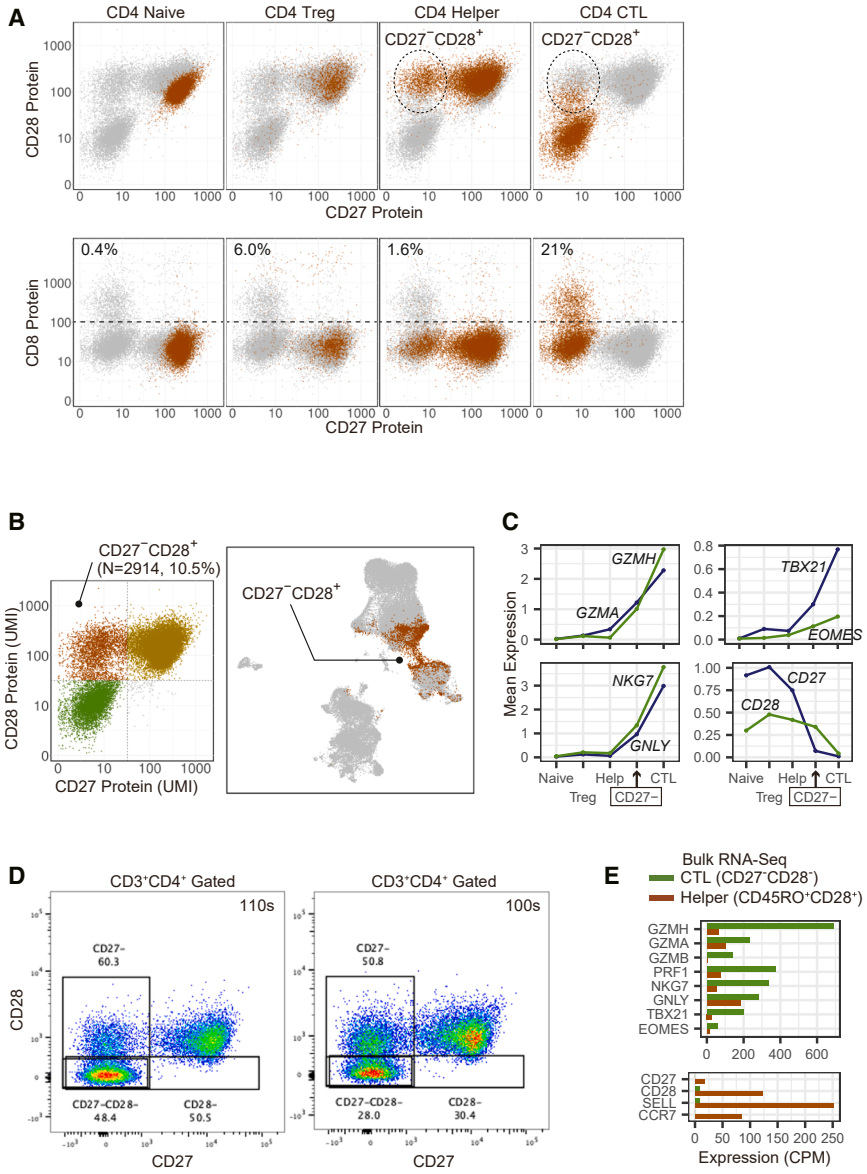

Figure 2. A transitional CD27⁻CD28⁺ state in CD4 T cells

(A) Protein expression of CD27, CD28, and CD8. CD4 subsets show a distinct CD27⁻CD28⁺ population (circled) in the helper and CTL clusters. CD8 is co-expressed at intermediate levels in 21% of CD4 CTLs.

(B) Bridging position of CD27⁻CD28⁺ cells. CD27⁻CD28⁺ cells (10.5% of CD4 T cells) are more frequent than CD27⁺CD28⁻ cells (<0.3%) and link helper and CTL clusters on UMAP.

(C) Mean expression of cytotoxic genes in CD27⁻CD28⁺ cells. CD27⁻CD28⁺ cells highlighted in the box show intermediate levels of cytotoxic markers (e.g., *GZMA*, *GZMH*) and transcription factors (e.g., *TBX21*, *EOMES*), reflecting their transitional state.

(D) Flow cytometry analysis of CD27 and CD28 expression in gated CD3⁺CD4⁺ T cells from a supercentenarian and a centenarian.

(E) Bulk RNA-seq analysis of FACS-sorted CTL (CD27⁻CD28⁻) and helper (CD45RO⁺CD28⁺) CD4 T cell subsets. Upper and lower panels show counts per million (CPM) for selected cytotoxic and transcription factor genes and surface-marker genes, respectively.

dual TCRs defined by Cell Ranger (10*x* Genomics), we remapped the raw sequencing reads onto the contigs. Our analysis confirmed that most cells had reads fully spanning the entire CDR3 region with an exact match. For example, the top clones of the supercentenarian samples C04 and C10 comprise 94 and 21 cells, respectively. Each clone contains two distinct beta chains, both of which are supported by the reads in over 95% of the cells (Figure 3C). The presence of dual alpha chains in samples A03, A04, and B02 was confirmed in the same way (Figure S3D). Importantly, dual TCRs were not exclusively found in CD4 CTLs; dual alpha and dual beta TCRs accounted for 7.6% and 2.0%, respectively, of the analyzed T cells (Figures 3D and S3E). Therefore, their functional relevance to clonal expansion remains uncertain.

Please cite this article in press as: Hashimoto et al., CD4 CTLs in supercentenarians: Signs of adaptive expansion in healthy aging, Cell Reports (2026), https://doi.org/10.1016/j.celrep.2026.117728

CellPress
OPEN ACCESS

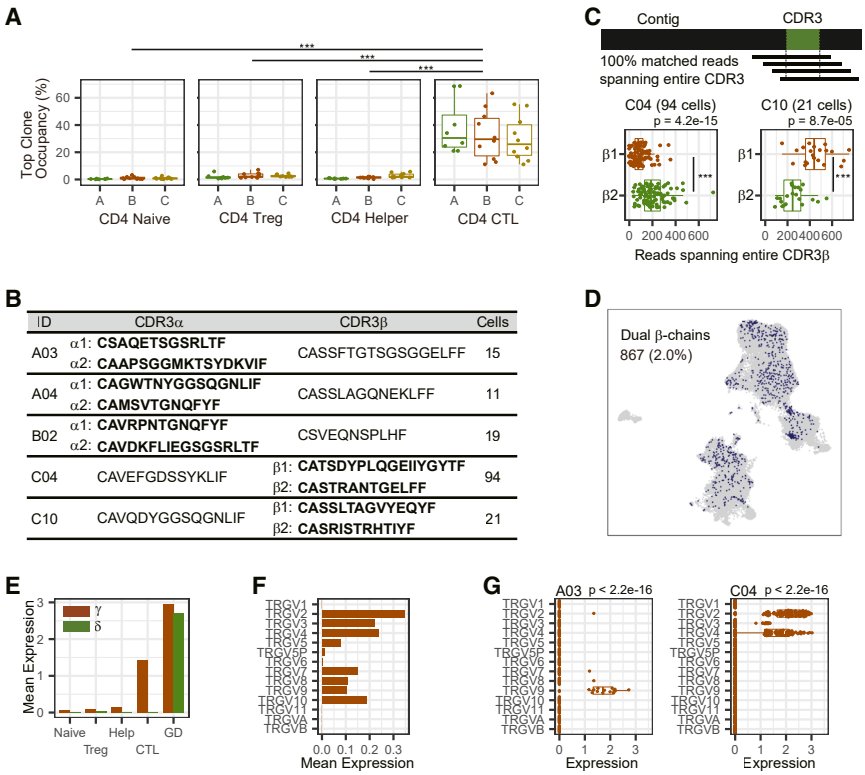

Figure 3. Non-canonical TCR features in CD4 CTLs

(A) Top clone occupancy in the 70s–90s age group (group A, $n = 8$), centenarians (group B, $n = 10$), and supercentenarians (group C, $n = 10$). Top clones of CD4 CTLs occupy an average of 33.3%. A Kruskal–Wallis test showed significant differences across the four CD4 subsets ($p < 2.2 \times 10^{-16}$), followed by Dunn's post hoc test with Bonferroni correction. Significant comparisons are marked (***$p < 0.001$).

(B) Dual TCR chains in top clones. Three clones exhibit dual TCR alpha chains, and two display dual TCR beta chains.

(C) Validation of dual beta chains. Read counts fully spanning the CDR3β region confirm two distinct beta chains in the top clones from supercentenarian samples C04 and C10. The counts were compared using the Wilcoxon rank-sum test (***$p < 0.001$).

(D) Distribution of dual beta chains. Dual beta chains account for 2.0% of T cells, shown on UMAP.

(E) Mean expression of TCRγ (red) and TCRδ (green) genes in five T cell subtypes. CD4 CTLs express TCRγ genes at approximately half the level of γδ T cells.

(F) Mean expression of 14 individual TCRγ genes in CD4 CTLs.

(G) Single-cell expression of TCRγ genes in top clones. The top clone from A03 predominantly expressed TRGV9, whereas the top clone from C04 co-expressed TRGV2 and TRGV4, illustrating inter-clonal variation. A Kruskal–Wallis test showed significant differences across the TRGV genes ($p < 2.2 \times 10^{-16}$). Boxplots: center, median; hinges, 25th/75th percentiles; whiskers, 1.5 × IQR. Dots: each donor (A) or cell (C and G).

In general, TCRγ and δ genes are not expressed in CD4 T cells because they are either rearranged or transcriptionally silenced during differentiation into αβ T cells.[37] Despite this typical suppression, we identified TCRγ gene expression in CD4 CTLs at approximately half the level seen in γδ T cells, whereas TCRδ genes remained undetected (Figure 3E). Given that several TCRγ V genes were expressed in the population of CD4 CTLs (Figure 3F), we further investigated whether individual top clones uniformly express the same *TCRγ V* genes at the single-cell level. Our analysis revealed that whereas some clones expressed a single *TCRγ V* gene, others co-expressed two distinct *TCRγ V* genes (Figure S3F). For example, *TRGV9* was dominant in the top clone from A03, whereas *TRGV2* and *TRGV4* were co-expressed in the top clone from C04 (Figure 3G). Altogether, CD4 CTLs exhibit a non-canonical TCR repertoire characterized by clonal expansion, dual TCR expression, and the activation of TCRγ genes, distinguishing them from typical CD4 T cells.

Potential expansion of CD4 CTLs in the cancer microenvironment

To investigate the potential antigenic targets of CD4 CTLs, we searched public TCR databases using the CDR3 sequences from the top clones listed in Figures 3B and S3C. In VDJdb, which is a curated database linking CDR3 sequences with known antigen specificities,[38] none of our CDR3α and CDR3β sequences were found among the 93,976 entries. This suggests that the top CD4 CTL clones may recognize antigens that are not well documented. We then expanded our search to TCRdb2.0,[39] a much larger database that contains over 690 million CDR3β sequences from 19,701 healthy and diseased samples (Figure 4A), although it does not include CDR3α sequences or information on antigen specificities. We identified 617 entries with CDR3β sequences that exactly matched those from the top clones in our samples (Figure S4A). Each entry provides sample information and a clonal frequency value, indicating the relative abundance of

Please cite this article in press as: Hashimoto et al., CD4 CTLs in supercentenarians: Signs of adaptive expansion in healthy aging, Cell Reports (2026), https://doi.org/10.1016/j.celrep.2026.117728

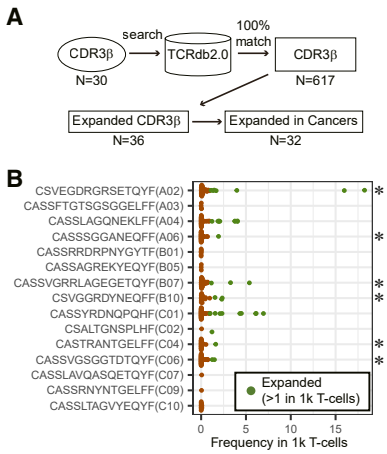

C

ID	CDR3β	Age	Condition	Tissue	Freq
A02	CSVEGDRGRSETQYF	82	NSCLC	Tumor	4.0
				Tumor-Adj	1.7
		NA	NSCLC	Tumor	18.2
		68	NSCLC	Tumor	1.5
		NA	NSCLC	Tumor-Adj	16.0
		48	NSCLC	Blood	1.1
		45	Healthy	Blood	1.3
A06	CASSSGGANEQFF	48	NSCLC	Tumor	1.9
B07	CASSVGRRLAGEGETQYF	74	NSCLC	Tumor-Adj	5.4
		62	NSCLC	Tumor-Adj	3.3
		83	NSCLC	Tumor-Adj	1.1
B10	CSVGGRDYNEQFF	68	NSCLC	Tumor	1.6
				Tumor-Adj	2.3
		69	NSCLC	Tumor-Adj	2.4
C04	CASTRANTGELFF	NA	NSCLC	Tumor	1.6
C06	CASSVGSGGTDTQYF	NA	NSCLC	Tumor	1.5
		NA	NSCLC	Tumor	1.2

NSCLC: Non-Small Cell Lung Cancer
Freq: Number of sequences per 1,000 T-cells, Adj: Adjacent

Figure 4. Top CD4 CTL clones matched cancer-associated CDR3β sequences in the TCRdb2.0 database

(A) CDR3β sequences from top CD4 CTL clones were searched in the TCRdb2.0 database, resulting in 617 matches.

(B) 36 clones were identified as expanded (>1 in 1,000 T cells), marked as green dots. Asterisks (*) indicate clones detailed in Figure 4C; clones without asterisks are detailed in Figure S4B.

(C) Detailed information on expanded clones marked with asterisks in B. The table summarizes CDR3β sequence, donor age, condition, tissue of origin, and frequency extracted from the database. Notably, these clones were frequently observed in NSCLC (non-small cell lung cancer) tumors or adjacent tissues.

the CDR3β in the sample. By applying a clonal frequency threshold of 0.1%, we found that 36 of the 617 entries were clonally expanded in their respective samples (Figure 4B). Notably, 32 of these entries originated from samples from patients with cancer. Specifically, 17 were from NSCLC, nine breast cancer, and six hepatocellular carcinoma samples, and the remaining entries were from two healthy samples and two other conditions (Figures 4C and S4B). For example, the CDR3β sequence CSVEGDRGRSETQYF, the top clone in sample A02, was identified across tumor tissues, adjacent tissues, and blood from five different patients with NSCLC. Similarly, CDR3β sequences from samples B07, B10, and C06 were observed in multiple NSCLC cases, whereas the sequence from A04 appeared in patients with multiple breast cancer. Nevertheless, none of the centenarians and supercentenarians in this study had any known history of NSCLC, breast cancer, or hepatocellular carcinoma. In addition, none had autoimmune diseases or Parkinson's disease. One supercentenarian had a history of skin cancer, and two centenarians had dementia, although Alzheimer's disease could not be confirmed. This raises the possibility that the observed expansion of CD4 CTLs may reflect early immune responses triggered by subclinical conditions, rather than responses to clinically evident cancers.

Functional convergence and clonal divergence of CD4 CTLs and CD8 TEMRA

To clarify similarities and differences between CD4 CTLs and CD8 T cells, we analyzed the two CD8 clusters, TEM and TEMRA, identified in Figure 1B, excluding a small donor-specific TEMRA cluster. As we previously noted, a fraction of CD4 CTLs express CD8. However, their CD8 levels remained at mid-range, clearly lower than those of bona fide CD8 T cells (Figures S5A and S5B). Importantly, these CD4 CTLs expressed *CD8A* but not *CD8B* (Figure S5C), suggesting that they are distinct from conventional CD8 T cells.

As shown above, CD4 CTLs represent a highly differentiated state, which is expected to resemble CD8 TEMRA, the terminally differentiated CD8 T cells, rather than TEM. Indeed, CD8 TEMRA exhibited high expression of cytotoxic genes and loss of CCR7, CD27, and CD28, a phenotype largely comparable to CD4 CTLs (Figures 5A and S5D). Unlike CD8 TEMRA, CD4 CTLs largely retained CD45RO expression without strong RA re-expression (Figure S5E). Another notable difference was in their differentiation trajectory. In CD4 CTLs, the major intermediate was $CD27^{-}CD28^{+}$ cells, whereas $CD27^{+}CD28^{-}$ cells were extremely rare (0.3%). By contrast, both CD8 TEM and TEMRA contained a substantial fraction of $CD27^{+}CD28^{-}$ cells (9.3% and 12%, respectively), indicating that in CD8 T cells the loss of CD28 can precede that of CD27 (Figure S5F).

It is well established that CD8 TEMRA cells increase with age and undergo clonal expansion.[40] In line with this, we observed a higher proportion of TEMRA cells in older age groups ($p = 0.001$, Jonckheere-Terpstra test) (Figure S5G). Their TCR repertoires also displayed signs of clonal expansion, with elevated Simpson's index values and increased top clone occupancy (Figure S5H), similar to what we observed in CD4 CTLs. A key question was whether CD4 CTLs and CD8 TEMRA cells expand in a coordinated manner in response to common antigens. However, no significant correlation was observed between the degree of expansion across individuals (Figure 5B). These findings suggest that the two subsets do not necessarily expand in concert, but are likely driven by distinct persistent antigens.

Analysis of top clonotypes further highlighted this difference. Whereas CD4 CTL top clones were entirely private, CD8 TEMRA contained several public clonotypes that were shared among independent donors (Figure 5C). This indicates that CD8 TEMRA cells are more likely to be driven by common antigens. Database searches yielded only limited matches: no exact αβ pair in VDJdb, only a few single-chain matches (Figure S5I), and 486 hits in TCRdb2.0, of which eight showed clonal

Please cite this article in press as: Hashimoto et al., CD4 CTLs in supercentenarians: Signs of adaptive expansion in healthy aging, Cell Reports (2026), https://doi.org/10.1016/j.celrep.2026.117728

CellPress
OPEN ACCESS

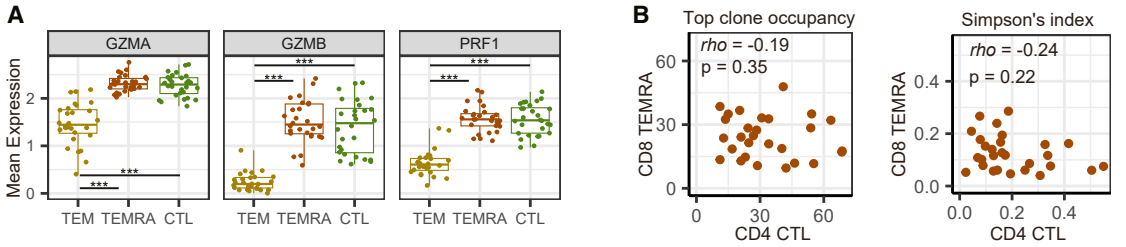

C

Expanded Public TCR1

ID	CDR3α	CDR3β	Cells
A05	CAVGALNNNDMRF	CASSPRVGAGGELFF	32
B10	CAVGALNNNDMRF	CASSPRVGAGGELFF	22
C08	CAVGALNNNDMRF	CASSQRAGAGGELFF	109
B01	CAVGALNNNDMRF	CASSDRTGAGGRLFF	63

Expanded Public TCR2

ID	CDR3α	CDR3β	Cells
A02	CAASYFGNEKLTF	CASSSASGGNEQFF	38
C04	CAASYFGNEKLTF	CASSSPTGGNEQFF	94

Figure 5. Distinct Clonal Expansion in CD8 TEMRA Compared to CD4 CTLs

(A) Expression of cytotoxic genes across CD8 TEM, CD8 TEMRA, and CD4 CTL subsets. Each dot represents the mean expression per individual within each subset. A Kruskal–Wallis test showed significant differences across three subsets ($p < 2.2 \times 10^{-16}$), followed by Dunn's post hoc test with Bonferroni correction. Significant pairwise comparisons are indicated (***$p < 0.001$).

(B) Comparison of clonal expansion between CD4 CTLs and CD8 TEMRA. Top clone occupancy and Simpson's index were compared between CTLs and TEMRA cells across individuals. No significant Spearman's correlation (rho) was observed.

(C) Public clonotypes expanded in CD8 TEMRA cells. Each table shows the donor ID and paired CDR3α and CDR3β sequences. Identical amino acid residues across donors are highlighted. TCR1 was shared as identical or highly similar sequences among four individuals, whereas TCR2 showed similar sequences between two individuals. Boxplots: center, median; hinges, 25th/75th percentiles; whiskers, 1.5 × IQR. Dots: each donor (A).

expansion (Figure S5J). Thus, while CD8 TEMRA display public clonotypes, their precise antigenic targets remain to be determined.

Diverse cytokine production within the same CD4 CTL clones

To gain insights into the function of CD4 CTLs, we performed secondary single-cell analysis on six samples, two from each age group (Figure 6A). In each sample, the cells were split into two conditions: stimulated with PMA and ionomycin and unstimulated controls. As in the primary analysis, transcriptome, surface proteins, and TCR sequences were profiled. After filtering, 6,400 T cells were compiled and divided into eight distinct clusters based on the transcriptome and surface protein profiles. The clusters were grouped into two major categories: $CD69^+$ activated and $CD69^-$ quiescent cells (Figure 6B), corresponding to the stimulated and unstimulated conditions, respectively (Figure S6A). Each of these groups contained four clusters: CD4 naive, Helper, CTL, and CD8 T cells (Figures 6B and S6B).

We confirmed the presence of $CD27^-CD28^+$ intermediate cells in both the activated and quiescent states (Figure S6C), in line with the primary dataset. Similarly, $CD8^+$ subsets were observed within the CD4 CTL populations under both conditions (Figures 6C and S6D). CD4 expression levels were reduced in activated CD4 T cells, as expected during T cell activation.[41] We compared the expression of cytotoxic genes between activated and quiescent CD4 CTL clusters and found that *GZMB* and *PRF1* were upregulated in the activated cells, whereas *GZMA* and *GZMH* were downregulated (Figure 6D). In addition, the expression of inflammatory cytokines IFN-γ and TNF-α was elevated in the activated CD4 CTL population. Consistently, pathway analysis using PROGENy[42] showed increased activity of NF-κB, MAPK, and PI3K signaling, further supporting the activated state of these cells (Figure S6E). Taking these results together, activated CD4 CTLs appear to possess cytotoxic potential through the GZMB pathway and robust pro-inflammatory activity.

To investigate the diversity of cytokine production among activated CD4 CTLs, we performed subclustering analysis using only the interleukin (IL) genes. Specifically, we analyzed the expression of all 43 ILs listed in the KEGG database.[43] Among them, 28 ILs were detected in the activated CD4 CTL cluster (Figure S7A). We identified eight clusters (Figure S7B), each characterized by the expression of specific ILs (Figure 7A). Among the eight clusters, subtype 2 was characterized by high expression of IL-4 and IL-13 (Figure 7B), both of which are hallmarks of Th2 cells, indicating the presence of a Th2-like population. In contrast, subtype 3 exhibited elevated levels of IL-21 (Figure S7C), a cytokine primarily produced by T follicular helper (Tfh) cells, which modulates B cell responses and enhances cytotoxic T cell activity.[44] Subtype 7 displayed higher expression of IL-10, a cytokine associated with immune suppression, whereas subtype 8 was distinguished by the expression of IL-31, which is linked to inflammatory responses, particularly in the skin.[45] Despite these differences in specific IL expression, all clusters shared high levels of IFN-γ and TNF-α (Figure S7D), indicating a common cytotoxic potential among the CD4 CTLs.

We then examined whether the highly expanded clones were restricted to specific subclusters or distributed across multiple subclusters. To address this, we first identified the largest clones within the activated CD4 CTLs. Similar to the primary analysis, we found highly expanded clones, with the top clone consisting of 68 of the 497 cells (Figure S7E). Four of the top five clones were also the most expanded in the primary analysis, indicating consistent clonal dominance within the same donors (Figures 3B and S3C). As shown in Figure 7C, the top five clones were

Please cite this article in press as: Hashimoto et al., CD4 CTLs in supercentenarians: Signs of adaptive expansion in healthy aging, Cell Reports (2026), https://doi.org/10.1016/j.celrep.2026.117728

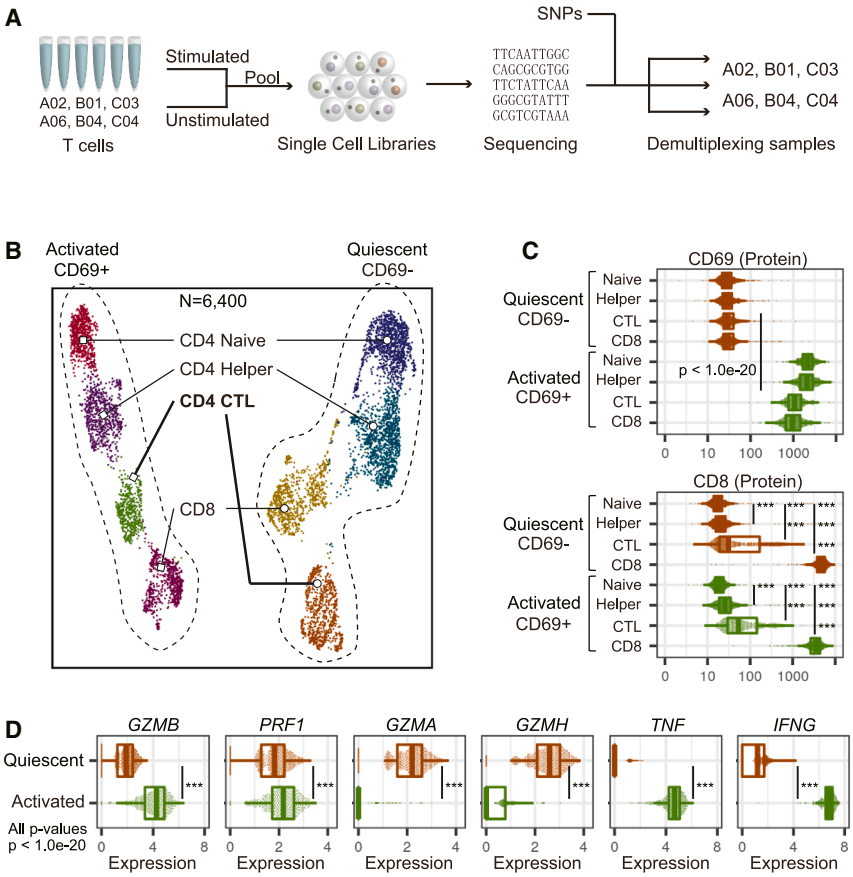

Figure 6. Characteristics of activated CD4 CTLs

(A) Workflow for secondary single-cell analysis of T cells. T cells from six samples (A02, A06, B01, B04, C03, C04) were pooled after stimulation with PMA and ionomycin (Stimulated) or left unstimulated (Unstimulated). Single-cell libraries were sequenced, and SNP-based demultiplexing was used to assign cells to their original donors.

(B) UMAP projection of T cells split by activation state. T cells (n = 6,400) are grouped into activated ($CD69^+$) and quiescent ($CD69^-$) states, outlined with dashed lines. Clusters correspond to major T cell subsets: CD4 naive, CD4 helper, CD4 CTLs, and CD8 T cells.

(C) Protein expression of CD69 and CD8 across T cell subsets. Expression levels of CD69 (top) and CD8 (bottom) are shown for activated and quiescent clusters. CD69 expression was compared between $CD69^-$ and $CD69^+$ cells using a Wilcoxon rank-sum test ($p < 1.0 \times 10^{-20}$). CD8 expression was analyzed using the Kruskal–Wallis test across the four subsets within $CD69^-$ and $CD69^+$ clusters, respectively (both $p < 2.2 \times 10^{-16}$). Dunn's post hoc test with Bonferroni correction identified significant differences among all pairs (***$p < 0.001$).

(D) Expression levels of cytotoxic and inflammatory genes in CD4 CTLs under activated and quiescent conditions, compared using the Wilcoxon rank-sum test (***$p < 0.001$). Boxplots: center, median; hinges, 25th/75th percentiles; whiskers, 1.5 × IQR. Dots: each cell (C and D).

distributed across multiple subclusters, rather than being confined to a single subcluster. For example, cells from Rank 1 were present in all subclusters, with a relatively high proportion (35%) in subcluster 2, whereas Rank 4 and Rank 5 showed 0% in this subcluster. These findings suggest that clones sharing the same TCR are not restricted to a single cytokine profile after activation.

DISCUSSION

CD4 CTLs have remained largely unexplored due to their low frequency and their discrepancy with conventional T cell classifications. In this study, we conducted integrated single-cell profiling of T cells, combining transcriptome, surface protein, and TCR sequence data across different age groups, including rare cohorts of centenarians and supercentenarians. This approach enabled us to distinguish CD4 CTLs from other subsets and to characterize their unique TCR repertoires and clonal dynamics. We observed an increase in CD4 CTLs emerging in later stages of aging, with substantial clonal proliferation in supercentenarians as well as in certain individuals under 100 years. TCR analysis of these expanded clones revealed non-canonical features, including γ chain activation and dual TCR expression. These observations raised the question of the underlying mechanisms driving the increase in CD4 CTLs during aging.

We hypothesized that the increase in CD4 CTLs reflects an adaptive response to persistent antigens that express MHC class II. These antigens are rare and may primarily emerge in the late stages of life. Several lines of evidence support this hypothesis. First, CD4 CTLs were clonally expanded across all

Please cite this article in press as: Hashimoto et al., CD4 CTLs in supercentenarians: Signs of adaptive expansion in healthy aging, Cell Reports (2026), https://doi.org/10.1016/j.celrep.2026.117728

CellPress
OPEN ACCESS

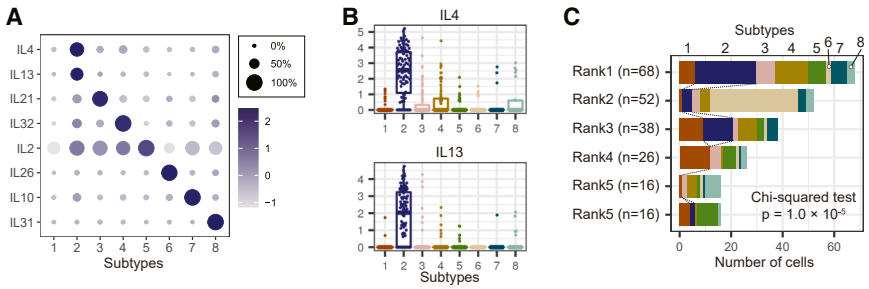

Figure 7. Diversity in cytokine expression defining subtypes of activated CD4 CTLs

(A) Cytokine expression profiles across CD4 CTL subtypes. Activated CD4 CTLs were categorized into eight subtypes based on the expression of interleukin (IL) genes. The size of the dots indicates the proportion of cells expressing each cytokine, while the color intensity represents the relative expression level of the cytokine within each subtype.

(B) Expression of IL-4 and IL-13 across CD4 CTL subtypes. Boxplots show the expression levels of IL-4 (top) and IL-13 (bottom) in each subtype. Subtype 2 exhibits the highest expression of both IL-4 and IL-13, indicating a Th2-like functional profile.

(C) Distribution of major expanded CD4 CTL clones across subtypes. The top five expanded clones (Rank 1 to Rank 5) are distributed across the eight CD4 CTL subtypes. Each bar represents the number of cells from a specific clone within each subtype, showing that clones are not confined to a single subtype. Subtype composition differs significantly among clonotypes (chi-squared test with simulated p value; $p = 1.0 \times 10^{-5}$). Boxplots: center, median; hinges, 25th/75th percentiles; whiskers, 1.5 × IQR. Dots: each cell (B).

samples, suggesting that repeated antigen exposure is involved in CD4 CTL expansion. Second, CD4 CTLs showed a stepwise loss of CD27 and CD28, progressing through a $CD27^{-}CD28^{+}$ intermediate state, with a subset gaining CD8 expression, indicating advanced differentiation. Nevertheless, they remained PD-1 negative, implying differentiation without exhaustion, in response to persistent antigen exposure. Third, our study identified distinct subtypes within identical CD4 CTL clones based on their IL profiles (Figure 7). This diversity within clonal populations suggests that CD4 CTLs adapt their cytokine responses to specific immune environments. Fourth, our top TCR clones matched TCRβ sequences from patients with cancer in a TCR database. Specifically, the top TCRβ sequences from six individuals, including healthy supercentenarians with no history of cancer, matched those in 14 patients with NSCLC (Figure 4C). Supporting this observation, CD4 CTLs have been reported to localize near MHC class II-positive tumor cells in patients with NSCLC[46] and to suppress tumor growth in mouse models.[19] Furthermore, a recent study identified GPR56 as a key marker for CD4 CTLs in lung cancer, revealing that these cells upregulate PD-1 and become exhausted.[34] Our CD4 CTLs also expressed *ADGRG1* (GPR56) (Figure S2D), but remained PD-1-negative (Figure S2C). This suggests these cells avoid exhaustion and may contribute to tumor immunosurveillance. Finally, CD4 CTLs have been reported to target other sources of persistent antigens, including senescent cells and latent viruses.[23,47] A study has demonstrated that CD4 CTLs eliminate senescent cells in aged human skin.[23] In this process, cellular senescence reactivates latent cytomegalovirus, leading CD4 CTLs to eliminate the senescent cells in an MHC class II-dependent manner. These findings suggest that CD4 CTLs may serve not only as markers of persistent MHC class II-positive antigens, but also as potential effectors for eliminating such antigens that accumulate with aging. Conversely, it is important to note that CD4 CTL expansion may also be associated with pathogenic effects. Aberrant accumulation of CD4 CTLs has been widely implicated in autoimmune diseases, cardiovascular diseases, and excessive inflammation.[48–50] Thus, CD4 CTLs likely act as a double-edged sword during aging, mediating either beneficial immunosurveillance or pathogenic tissue damage depending on the degree of inflammatory control. Translationally, identifying their precise targets could guide the development of targeted therapies to manage subclinical tumors or latent infections in the elderly.

The increase in CD4 CTLs likely reflects a restructuring of the T cell repertoire that occurs with aging. This restructuring can be described as a shift in primary immune targets, moving from diverse antigens to learned antigens and finally to persistent antigens in advanced age. In youth, high TCR diversity allows the immune system to respond to a wide range of antigens in its environment, while forming immunological memory. At the same time, thymic involution reduces the production of naive T cells, leading to a gradual prioritization of previously encountered antigens.[51] Although this shift reduces the capacity to address new antigens due to declining TCR diversity,[52] it reflects a rational process, allowing the immune system to focus on experienced antigens. This transition must have a benefit, because thymic involution is evolutionarily conserved across vertebrates.[53] In advanced age, the immune system faces an increased prevalence of persistent antigens, most commonly processed via MHC class I molecules and recognized by CD8 T cells.[54] However, a distinct subset of these antigens, originating from tumors, senescent cells, and reactivated latent viruses, is presented through MHC class II molecules, enabling recognition by CD4 CTLs.[20,23] Our analysis confirmed that CD8 TEMRA cells also increase with age and undergo clonal expansion. However, unlike CD4 CTLs, their top clonotypes included public sequences shared among donors, and the degree of expansion was not correlated between the two subsets. These findings suggest that CD8 TEMRA expansion is likely driven by common antigens, whereas CD4 CTLs reflect more individualized responses to MHC class II-restricted antigens. The expansion of CD4 CTLs becomes evident only around the age of 100, aligning with the period when persistent antigens are

abundant. This temporal correlation suggests that the increase in CD4 CTLs represents an adaptive strategy to address persistent challenges in aging immunity. This adaptation demonstrates the notable plasticity of CD4 T cells, enabling a shift toward persistent antigens at the population level and a transition from helper to cytotoxic roles at the cellular level.

Limitations of the study

A key limitation of this study is the lack of direct functional validation *in vivo*. First, our analysis focused on circulating T cells, leaving their actual tissue-specific functions unresolved, including the specific cells or antigens they target and eliminate. Future studies incorporating tissue-resident immune cells will be essential to address this gap. Second, the TCR database matches were based solely on CDR3β sequences. They should be interpreted as exploratory evidence of overlap with previously reported TCR repertoires rather than evidence that these TCRs recognize the same antigen. Third, due to the technical challenges of isolating primary cells from supercentenarians, our functional insights rely on *ex vivo* stimulation experiments. Thus, how these CD4 CTLs and their specific cytokine profiles directly contribute to healthy aging requires further experimental elucidation. Finally, the extreme rarity of the subjects resulted in a relatively small cohort size. Although consistent trends were observed, individual variations could influence the results, highlighting the need for larger cohorts in future studies.

RESOURCE AVAILABILITY

Lead contact

Requests for further information and resources should be directed to and will be fulfilled by the lead contact, Kosuke Hashimoto (kosuke.hashimoto@protein.osaka-u.ac.jp).

Materials availability

This study did not generate new unique reagents.

Data and code availability

- Raw sequencing data have been deposited in the NBDC Human Database under the accession ID hum0511 and in the Genomic Expression Archive (GEA) under accession IDs E-GEAD-1107 and E-GEAD-1108. They are available under controlled access, subject to approval by the NBDC Data Access Committee.
- Processed single-cell RNA-seq data from primary (Dataset 1) and secondary (Dataset 2) analyses are freely available in the Osaka University Knowledge Archive (OUKA) via https://hdl.handle.net/11094/104062. Each dataset includes standard output files (barcodes.tsv.gz, features.tsv.gz, matrix.mtx.gz, and clonotypes.csv) generated using Cell Ranger v6.1.2.
- All original code and the pretrained VAE model are freely available in the same OUKA record.
- Any additional information required to reanalyze the data reported in this paper is available from the lead contact upon request.

ACKNOWLEDGMENTS

We sincerely thank all the donors, especially the supercentenarians and centenarians, whose invaluable contributions made this study possible. We also thank Tsukasa Kouno and Norihito Hayatsu for technical assistance with the single-cell experiments and sequencing. This work was supported by JSPS KAKENHI grant nos. JP21K06135 and JP24K09423, the Promotion Program for Frontier Protein Research from the Institute for Protein Research, The University of Osaka, Takeda Science Foundation, The Mochida Memorial Foundation for Medical and Pharmaceutical Research, Research Grants for Keio University Global Initiative Research Projects, and a Research Grant from MEXT to the RIKEN Center for Integrative Medical Sciences.

AUTHOR CONTRIBUTIONS

Conceptualization, K.H., Y.A., P.C., and N.H.; methodology, K.H., M.K.-I., H.I., M.T., and K.I.; investigation, K.H., M.K.-I., H.I., and K.I.; resources, T.S., N.H., and Y.A.; writing – original draft, K.H.; writing – review and editing, all authors; funding acquisition, K.H., Y.A., P.C., and N.H.; supervision, K.M., Y.O., I.T., K.I., P.C., N.H., and Y.A.

DECLARATION OF INTERESTS

The authors declare no competing interests.

DECLARATION OF GENERATIVE AI AND AI-ASSISTED TECHNOLOGIES IN THE WRITING PROCESS

During the preparation of this work, the authors used ChatGPT (OpenAI) and Gemini (Google) to assist with language editing. After using these tools, the authors reviewed and edited the content as needed and take full responsibility for the content of the publication.

STAR★METHODS

Detailed methods are provided in the online version of this paper and include the following:

- KEY RESOURCES TABLE
- EXPERIMENTAL MODEL AND STUDY PARTICIPANT DETAILS
- METHOD DETAILS
  - Isolation of T cells from human blood samples
  - Labeling of cell surface proteins
  - Preparation of single-cell transcriptome, cell surface protein, and TCR libraries
  - Processing of the primary single-cell sequence data
  - PMA and ionomycin stimulation for secondary single-cell analysis
  - Processing of the secondary single-cell sequence data
  - Flow cytometry, cell sorting, and bulk RNA-seq
  - Prediction of CD4 CTLs in public datasets
- QUANTIFICATION AND STATISTICAL ANALYSIS

SUPPLEMENTAL INFORMATION

Supplemental information can be found online at https://doi.org/10.1016/j.celrep.2026.117728.

Received: March 26, 2025
Revised: May 1, 2026
Accepted: July 6, 2026

REFERENCES

1. Guo, J., Huang, X., Dou, L., Yan, M., Shen, T., Tang, W., and Li, J. (2022). Aging and aging-related diseases: from molecular mechanisms to interventions and treatments. Signal Transduct. Targeted Ther. *7*, 391. https://doi.org/10.1038/s41392-022-01251-0.
2. Amorim, J.A., Coppotelli, G., Rolo, A.P., Palmeira, C.M., Ross, J.M., and Sinclair, D.A. (2022). Mitochondrial and metabolic dysfunction in ageing and age-related diseases. Nat. Rev. Endocrinol. *18*, 243–258. https://doi.org/10.1038/s41574-021-00626-7.
3. Liu, Z., Liang, Q., Ren, Y., Guo, C., Ge, X., Wang, L., Cheng, Q., Luo, P., Zhang, Y., and Han, X. (2023). Immunosenescence: molecular

mechanisms and diseases. Signal Transduct. Targeted Ther. *8*, 200. https://doi.org/10.1038/s41392-023-01451-2.

4. Wang, Y., Dong, C., Han, Y., Gu, Z., and Sun, C. (2022). Immunosenescence, aging and successful aging. Front. Immunol. *13*, 942796. https://doi.org/10.3389/fimmu.2022.942796.
5. Yousefzadeh, M.J., Flores, R.R., Zhu, Y., Schmiechen, Z.C., Brooks, R.W., Trussoni, C.E., Cui, Y., Angelini, L., Lee, K.A., McGowan, S.J., et al. (2021). An aged immune system drives senescence and ageing of solid organs. Nature *594*, 100–105. https://doi.org/10.1038/s41586-021-03547-7.
6. Zhu, H., Chen, J., Liu, K., Gao, L., Wu, H., Ma, L., Zhou, J., Liu, Z., and Han, J.D.J. (2023). Human PBMC scRNA-seq-based aging clocks reveal ribosome to inflammation balance as a single-cell aging hallmark and super longevity. Sci. Adv. *9*, eabq7599. https://doi.org/10.1126/sciadv.abq7599.
7. Hirata, T., Arai, Y., Yuasa, S., Abe, Y., Takayama, M., Sasaki, T., Kunitomi, A., Inagaki, H., Endo, M., Morinaga, J., et al. (2020). Associations of cardiovascular biomarkers and plasma albumin with exceptional survival to the highest ages. Nat. Commun. *11*, 3820. https://doi.org/10.1038/s41467-020-17636-0.
8. Komaki, S., Nagata, M., Arai, E., Otomo, R., Ono, K., Abe, Y., Ohmomo, H., Umekage, S., Shinozaki, N.O., Hachiya, T., et al. (2023). Epigenetic profile of Japanese supercentenarians: a cross-sectional study. Lancet Healthy Longev. *4*, e83–e90. https://doi.org/10.1016/S2666-7568(23)00002-8.
9. Sasaki, T., Tadaka, S., Hirata, T., Nishimoto, Y., Shikimoto, R., Abe, Y., Shiohama, A., Shirota, M., Motoike, I., Tamiya, G., et al. (2024). Genetic determinants of centenarian longevity, as quantified by the 'CentPGS' score, are associated with a lower risk of multiple age-related diseases and a longer healthspan. Research Square. https://doi.org/10.21203/rs.3.rs-3916561/v1.
10. Hashimoto, K., Kouno, T., Ikawa, T., Hayatsu, N., Miyajima, Y., Yabukami, H., Terooatea, T., Sasaki, T., Suzuki, T., Valentine, M., et al. (2019). Single-cell transcriptomics reveals expansion of cytotoxic CD4 T cells in supercentenarians. Proc. Natl. Acad. Sci. USA *116*, 24242–24251. https://doi.org/10.1073/pnas.1907883116.
11. Weng, N.P., Akbar, A.N., and Goronzy, J. (2009). CD28(-) T cells: their role in the age-associated decline of immune function. Trends Immunol. *30*, 306–312. https://doi.org/10.1016/j.it.2009.03.013.
12. Maly, K., and Schirmer, M. (2015). The story of CD4+ CD28- T cells revisited: solved or still ongoing? J. Immunol. Res. *2015*, 348746. https://doi.org/10.1155/2015/348746.
13. Elyahu, Y., Hekselman, I., Eizenberg-Magar, I., Berner, O., Strominger, I., Schiller, M., Mittal, K., Nemirovsky, A., Eremenko, E., Vital, A., et al. (2019). Aging promotes reorganization of the CD4 T cell landscape toward extreme regulatory and effector phenotypes. Sci. Adv. *5*, eaaw8330. https://doi.org/10.1126/sciadv.aaw8330.
14. Appay, V., Zaunders, J.J., Papagno, L., Sutton, J., Jaramillo, A., Waters, A., Easterbrook, P., Grey, P., Smith, D., McMichael, A.J., et al. (2002). Characterization of CD4(+) CTLs ex vivo. J. Immunol. *168*, 5954–5958. https://doi.org/10.4049/jimmunol.168.11.5954.
15. Malyshkina, A., Brüggemann, A., Paschen, A., and Dittmer, U. (2023). Cytotoxic CD4(+) T cells in chronic viral infections and cancer. Front. Immunol. *14*, 1271236. https://doi.org/10.3389/fimmu.2023.1271236.
16. Takeuchi, A., and Saito, T. (2017). CD4 CTL, a Cytotoxic Subset of CD4(+) T Cells, Their Differentiation and Function. Front. Immunol. *8*, 194. https://doi.org/10.3389/fimmu.2017.00194.
17. Zheng, N., Fujiwara, M., Ueno, T., Oka, S., and Takiguchi, M. (2009). Strong ability of Nef-specific CD4+ cytotoxic T cells to suppress human immunodeficiency virus type 1 (HIV-1) replication in HIV-1-infected CD4+ T cells and macrophages. J. Virol. *83*, 7668–7677. https://doi.org/10.1128/JVI.00513-09.
18. Meckiff, B.J., Ramírez-Suástegui, C., Fajardo, V., Chee, S.J., Kusnadi, A., Simon, H., Eschweiler, S., Grifoni, A., Pelosi, E., Weiskopf, D., et al. (2020). Imbalance of Regulatory and Cytotoxic SARS-CoV-2-Reactive CD4(+) T Cells in COVID-19. Cell *183*, 1340–1353.e16. https://doi.org/10.1016/j.cell.2020.10.001.
19. Ducellier, S., Demeules, M., Letribot, B., Gaetani, M., Michaudel, C., Sokol, H., Hamze, A., Alami, M., Nascimento, M., and Apcher, S. (2024). Dual molecule targeting HDAC6 leads to intratumoral CD4+ cytotoxic lymphocytes recruitment through MHC-II upregulation on lung cancer cells. J. Immunother. Cancer *12*, e007588. https://doi.org/10.1136/jitc-2023-007588.
20. Oh, D.Y., Kwek, S.S., Raju, S.S., Li, T., McCarthy, E., Chow, E., Aran, D., Ilano, A., Pai, C.C.S., Rancan, C., et al. (2020). Intratumoral CD4(+) T Cells Mediate Anti-tumor Cytotoxicity in Human Bladder Cancer. Cell *181*, 1612–1625.e13. https://doi.org/10.1016/j.cell.2020.05.017.
21. Cachot, A., Bilous, M., Liu, Y.C., Li, X., Saillard, M., Cenerenti, M., Rockinger, G.A., Wyss, T., Guillaume, P., Schmidt, J., et al. (2021). Tumor-specific cytolytic CD4 T cells mediate immunity against human cancer. Sci. Adv. *7*, eabe3348. https://doi.org/10.1126/sciadv.abe3348.
22. Lin, W., Singh, V., Springer, R., Choonoo, G., Gupta, N., Patel, A., Frleta, D., Zhong, J., Owczarek, T., Decker, C., et al. (2023). Human CD4 cytotoxic T lymphocytes mediate potent tumor control in humanized immune system mice. Commun. Biol. *6*, 447. https://doi.org/10.1038/s42003-023-04812-3.
23. Hasegawa, T., Oka, T., Son, H.G., Oliver-García, V.S., Azin, M., Eisenhaure, T.M., Lieb, D.J., Hacohen, N., and Demehri, S. (2023). Cytotoxic CD4(+) T cells eliminate senescent cells by targeting cytomegalovirus antigen. Cell *186*, 1417–1431.e20. https://doi.org/10.1016/j.cell.2023.02.033.
24. Luo, O.J., Lei, W., Zhu, G., Ren, Z., Xu, Y., Xiao, C., Zhang, H., Cai, J., Luo, Z., Gao, L., et al. (2022). Multidimensional single-cell analysis of human peripheral blood reveals characteristic features of the immune system landscape in aging and frailty. Nat. Aging *2*, 348–364. https://doi.org/10.1038/s43587-022-00198-9.
25. Terekhova, M., Swain, A., Bohacova, P., Aladyeva, E., Arthur, L., Laha, A., Mogilenko, D.A., Burdess, S., Sukhov, V., Kleverov, D., et al. (2023). Single-cell atlas of healthy human blood unveils age-related loss of NKG2C(+)GZMB(-)CD8(+) memory T cells and accumulation of type 2 memory T cells. Immunity *56*, 2836–2854.e9. https://doi.org/10.1016/j.immuni.2023.10.013.
26. Wang, Y., Li, R., Tong, R., Chen, T., Sun, M., Luo, L., Li, Z., Chen, Y., Zhao, Y., Zhang, C., et al. (2025). Integrating single-cell RNA and T cell/B cell receptor sequencing with mass cytometry reveals dynamic trajectories of human peripheral immune cells from birth to old age. Nat. Immunol. *26*, 308–322. https://doi.org/10.1038/s41590-024-02059-6.
27. Gong, Q., Sharma, M., Glass, M.C., Kuan, E.L., Chander, A., Singh, M., Graybuck, L.T., Thomson, Z.J., LaFrance, C.M., Rachid Zaim, S., et al. (2025). Multi-omic profiling reveals age-related immune dynamics in healthy adults. Nature *648*, 696–706. https://doi.org/10.1038/s41586-025-09686-5.
28. Yazar, S., Alquicira-Hernandez, J., Wing, K., Senabouth, A., Gordon, M.G., Andersen, S., Lu, Q., Rowson, A., Taylor, T.R.P., Clarke, L., et al. (2022). Single-cell eQTL mapping identifies cell type-specific genetic control of autoimmune disease. Science *376*, eabf3041. https://doi.org/10.1126/science.abf3041.
29. Domínguez Conde, C., Xu, C., Jarvis, L.B., Rainbow, D.B., Wells, S.B., Gomes, T., Howlett, S.K., Suchanek, O., Polanski, K., King, H.W., et al. (2022). Cross-tissue immune cell analysis reveals tissue-specific features in humans. Science *376*, eabl5197. https://doi.org/10.1126/science.abl5197.
30. Hao, Y., Hao, S., Andersen-Nissen, E., Mauck, W.M., 3rd, Zheng, S., Butler, A., Lee, M.J., Wilk, A.J., Darby, C., Zager, M., et al. (2021). Integrated analysis of multimodal single-cell data. Cell *184*, 3573–3587.e29. https://doi.org/10.1016/j.cell.2021.04.048.
31. Thewissen, M., Somers, V., Hellings, N., Fraussen, J., Damoiseaux, J., and Stinissen, P. (2007). CD4+CD28null T cells in autoimmune disease: pathogenic features and decreased susceptibility to immunoregulation.

J. Immunol. *179*, 6514–6523. https://doi.org/10.4049/jimmunol.179.10.6514.

32. van Leeuwen, E.M.M., Remmerswaal, E.B.M., Vossen, M.T.M., Rowshani, A.T., Wertheim-van Dillen, P.M.E., van Lier, R.A.W., and ten Berge, I.J.M. (2004). Emergence of a CD4+CD28- granzyme B+, cytomegalovirus-specific T cell subset after recovery of primary cytomegalovirus infection. J. Immunol. *173*, 1834–1841. https://doi.org/10.4049/jimmunol.173.3.1834.
33. Xiong, Z., Gao, Y., He, J., Bahabayi, A., Zeng, X., Zhang, Z., Hasimu, A., Zhang, Y., Guo, S., Wang, P., and Liu, C. (2026). GPR56 Outperforms CD319 as a Discriminative Marker for CD4 (+) Cytotoxic T Lymphocytes and Is Elevated in Primary Sjogren's Syndrome. Immunology *177*, 713–724. https://doi.org/10.1111/imm.70073.
34. Liu, C., Liu, T., Hu, Y., Zeng, X., Alimu, X., Song, S., Lu, S., Song, Y., and Wang, P. (2023). G Protein-Coupled Receptor 56 Characterizes CTLs and Reflects the Progression of Lung Cancer Patients. J. Immunol. *211*, 683–692. https://doi.org/10.4049/jimmunol.2101048.
35. Lin, M., Chen, D., Shao, Z., Liu, Q., Hao, Z., Xin, Z., Chen, Y., Wu, W., Chen, X., He, T., et al. (2024). Inflammatory dendritic cells restrain CD11b(+)CD4(+) CTLs via CD200R in human NSCLC. Cell Rep. *43*, 113767. https://doi.org/10.1016/j.celrep.2024.113767.
36. Preglej, T., and Ellmeier, W. (2022). CD4(+) Cytotoxic T cells - Phenotype, Function and Transcriptional Networks Controlling Their Differentiation Pathways. Immunol. Lett. *247*, 27–42. https://doi.org/10.1016/j.imlet.2022.05.001.
37. Rodríguez-Caparrós, A., García, V., Casal, Á., López-Ros, J., García-Mariscal, A., Tani-Ichi, S., Ikuta, K., and Hernández-Munain, C. (2019). Notch Signaling Controls Transcription via the Recruitment of RUNX1 and MYB to Enhancers during T Cell Development. J. Immunol. *202*, 2460–2472. https://doi.org/10.4049/jimmunol.1801650.
38. Goncharov, M., Bagaev, D., Shcherbinin, D., Zvyagin, I., Bolotin, D., Thomas, P.G., Minervina, A.A., Pogorelyy, M.V., Ladell, K., McLaren, J.E., et al. (2022). VDJdb in the pandemic era: a compendium of T cell receptors specific for SARS-CoV-2. Nat. Methods *19*, 1017–1019. https://doi.org/10.1038/s41592-022-01578-0.
39. Chen, S.Y., Yue, T., Lei, Q., and Guo, A.Y. (2021). TCRdb: a comprehensive database for T-cell receptor sequences with powerful search function. Nucleic Acids Res. *49*, D468–D474. https://doi.org/10.1093/nar/gkaa796.
40. Zhang, H., Weyand, C.M., and Goronzy, J.J. (2021). Hallmarks of the aging T-cell system. FEBS J. *288*, 7123–7142. https://doi.org/10.1111/febs.15770.
41. Pelchen-Matthews, A., Parsons, I.J., and Marsh, M. (1993). Phorbol ester-induced downregulation of CD4 is a multistep process involving dissociation from p56lck, increased association with clathrin-coated pits, and altered endosomal sorting. J. Exp. Med. *178*, 1209–1222. https://doi.org/10.1084/jem.178.4.1209.
42. Schubert, M., Klinger, B., Klünemann, M., Sieber, A., Uhlitz, F., Sauer, S., Garnett, M.J., Blüthgen, N., and Saez-Rodriguez, J. (2018). Perturbation-response genes reveal signaling footprints in cancer gene expression. Nat. Commun. *9*, 20. https://doi.org/10.1038/s41467-017-02391-6.
43. Kanehisa, M., Furumichi, M., Sato, Y., Matsuura, Y., and Ishiguro-Watanabe, M. (2025). KEGG: biological systems database as a model of the real world. Nucleic Acids Res. *53*, D672–D677. https://doi.org/10.1093/nar/gkae909.
44. Isvoranu, G., and Chiritoiu-Butnaru, M. (2024). Therapeutic potential of interleukin-21 in cancer. Front. Immunol. *15*, 1369743. https://doi.org/10.3389/fimmu.2024.1369743.
45. Datsi, A., Steinhoff, M., Ahmad, F., Alam, M., and Buddenkotte, J. (2021). Interleukin-31: The "itchy" cytokine in inflammation and therapy. Allergy *76*, 2982–2997. https://doi.org/10.1111/all.14791.
46. Lau, D., Khare, S., Stein, M.M., Jain, P., Gao, Y., BenTaieb, A., Rand, T.A., Salahudeen, A.A., and Khan, A.A. (2022). Integration of tumor extrinsic and intrinsic features associates with immunotherapy response in non-small cell lung cancer. Nat. Commun. *13*, 4053. https://doi.org/10.1038/s41467-022-31769-4.
47. Narmada, B.C., Khakpoor, A., Shirgaonkar, N., Narayanan, S., Aw, P.P.K., Singh, M., Ong, K.H., Owino, C.O., Ng, J.W.T., Yew, H.C., et al. (2024). Single-cell landscape of functionally cured chronic hepatitis B patients reveals activation of innate and altered CD4-CTL-driven adaptive immunity. J. Hepatol. *81*, 42–61. https://doi.org/10.1016/j.jhep.2024.02.017.
48. Zuroff, L., Rezk, A., Shinoda, K., Espinoza, D.A., Elyahu, Y., Zhang, B., Chen, A.A., Shinohara, R.T., Jacobs, D., Alcalay, R.N., et al. (2022). Immune aging in multiple sclerosis is characterized by abnormal CD4 T cell activation and increased frequencies of cytotoxic CD4 T cells with advancing age. EBioMedicine *82*, 104179. https://doi.org/10.1016/j.ebiom.2022.104179.
49. Mattoo, H., Stone, J.H., and Pillai, S. (2017). Clonally expanded cytotoxic CD4(+) T cells and the pathogenesis of IgG4-related disease. Autoimmunity *50*, 19–24. https://doi.org/10.1080/08916934.2017.1280029.
50. Dumitriu, I.E., Araguás, E.T., Baboonian, C., and Kaski, J.C. (2009). CD4+ CD28 null T cells in coronary artery disease: when helpers become killers. Cardiovasc. Res. *81*, 11–19. https://doi.org/10.1093/cvr/cvn248.
51. Naylor, K., Li, G., Vallejo, A.N., Lee, W.W., Koetz, K., Bryl, E., Witkowski, J., Fulbright, J., Weyand, C.M., and Goronzy, J.J. (2005). The influence of age on T cell generation and TCR diversity. J. Immunol. *174*, 7446–7452. https://doi.org/10.4049/jimmunol.174.11.7446.
52. Britanova, O.V., Putintseva, E.V., Shugay, M., Merzlyak, E.M., Turchaninova, M.A., Staroverov, D.B., Bolotin, D.A., Lukyanov, S., Bogdanova, E.A., Mamedov, I.Z., et al. (2014). Age-related decrease in TCR repertoire diversity measured with deep and normalized sequence profiling. J. Immunol. *192*, 2689–2698. https://doi.org/10.4049/jimmunol.1302064.
53. Shanley, D.P., Aw, D., Manley, N.R., and Palmer, D.B. (2009). An evolutionary perspective on the mechanisms of immunosenescence. Trends Immunol. *30*, 374–381. https://doi.org/10.1016/j.it.2009.05.001.
54. Weiskopf, D., Weinberger, B., and Grubeck-Loebenstein, B. (2009). The aging of the immune system. Transpl. Int. *22*, 1041–1050. https://doi.org/10.1111/j.1432-2277.2009.00927.x.
55. Garrison, E., and Marth, G. (2012). Haplotype-based variant detection from short-read sequencing. arXiv, arXiv:1207.3907. https://doi.org/10.48550/arXiv.1207.3907.
56. Danecek, P., Auton, A., Abecasis, G., Albers, C.A., Banks, E., DePristo, M.A., Handsaker, R.E., Lunter, G., Marth, G.T., Sherry, S.T., et al. (2011). The variant call format and VCFtools. Bioinformatics *27*, 2156–2158. https://doi.org/10.1093/bioinformatics/btr330.
57. Kang, H.M., Subramaniam, M., Targ, S., Nguyen, M., Maliskova, L., McCarthy, E., Wan, E., Wong, S., Byrnes, L., Lanata, C.M., et al. (2018). Multiplexed droplet single-cell RNA-sequencing using natural genetic variation. Nat. Biotechnol. *36*, 89–94. https://doi.org/10.1038/nbt.4042.
58. Dobin, A., Davis, C.A., Schlesinger, F., Drenkow, J., Zaleski, C., Jha, S., Batut, P., Chaisson, M., and Gingeras, T.R. (2013). STAR: ultrafast universal RNA-seq aligner. Bioinformatics *29*, 15–21. https://doi.org/10.1093/bioinformatics/bts635.
59. Frankish, A., Carbonell-Sala, S., Diekhans, M., Jungreis, I., Loveland, J.E., Mudge, J.M., Sisu, C., Wright, J.C., Arnan, C., Barnes, I., et al. (2023). GENCODE: reference annotation for the human and mouse genomes in 2023. Nucleic Acids Res. *51*, D942–D949. https://doi.org/10.1093/nar/gkac1071.

Please cite this article in press as: Hashimoto et al., CD4 CTLs in supercentenarians: Signs of adaptive expansion in healthy aging, Cell Reports (2026), https://doi.org/10.1016/j.celrep.2026.117728

STAR★METHODS

KEY RESOURCES TABLE

REAGENT or RESOURCE	SOURCE	IDENTIFIER
Antibodies		
TotalSeq-C0251 anti-human Hashtag 1	BioLegend	Cat# 394661; clone LNH-94; 2M2
TotalSeq-C0253 anti-human Hashtag 3	BioLegend	Cat# 394665; clone LNH-94; 2M2
TotalSeq-C0255 anti-human Hashtag 5	BioLegend	Cat# 394669; clone LNH-94; 2M2
TotalSeq-C0034 anti-human CD3	BioLegend	Cat# 300479; clone UCHT1
TotalSeq-C0072 anti-human CD4	BioLegend	Cat# 300567; clone RPA-T4
TotalSeq-C0046 anti-human CD8	BioLegend	Cat# 344753; clone SK1
TotalSeq-C0063 anti-human CD45RA	BioLegend	Cat# 304163; clone HI100
TotalSeq-C0386 anti-human CD28	BioLegend	Cat# 302963; clone CD28.2
TotalSeq-C0087 anti-human CD45RO	BioLegend	Cat# 304259; clone UCHL1
TotalSeq-C0154 anti-human CD27	BioLegend	Cat# 302853; clone O323
TotalSeq-C0156 anti-human CD95 (Fas)	BioLegend	Cat# 305651; clone DX2
TotalSeq-C0582 anti-human TCR Vδ2	BioLegend	Cat# 331435; clone B6
TotalSeq-C0085 anti-human CD25	BioLegend	Cat# 302649; clone BC96
TotalSeq-C0148 anti-human CD197 (CCR7)	BioLegend	Cat# 353251; clone G043H7
TotalSeq-C0390 anti-human CD127 (IL-7Rα)	BioLegend	Cat# 351356; clone A019D5
TotalSeq-C0088 anti-human CD279 (PD-1)	BioLegend	Cat# 329963; clone EH12.2H7
TotalSeq-C0149 anti-human CD161	BioLegend	Cat# 339947; clone HP-3G10
TotalSeq-C0250 anti-mouse/human KLRG1 (MAFA)	BioLegend	Cat# 138433; clone 2F1/KLRG1
TotalSeq-C0047 anti-human CD56 (NCAM)	BioLegend	Cat# 362559; clone 5.1H11
TotalSeq-C0080 anti-human CD8A	BioLegend	Cat# 301071; clone RPA-T8
TotalSeq-C0146 anti-human CD69	BioLegend	Cat# 310951; clone FN50
Biological samples		
T-cell-enriched PBMCs from supercentenarians	This paper	N/A
T-cell-enriched PBMCs from centenarians	This paper	N/A
T-cell-enriched PBMCs from donors aged 70s–90s	This paper	N/A
Chemicals, peptides, and recombinant proteins		
Ficoll-Paque Plus	Cytiva	Cat# 17-1440-02
CELLBANKER 2	Takara Bio	Cat# CB031
Human TruStain FcX	BioLegend	Cat# 422301
Cell Stimulation Cocktail, PMA/Ionomycin	BioLegend	Cat# 423301
Brefeldin A Solution	eBioscience	Cat# 00-4506-51
Critical commercial assays		
SepMate-15 tubes	STEMCELL Technologies	Cat# 85415
RosetteSep Human T cell Enrichment Cocktail	STEMCELL Technologies	Cat# 15061
Nextera XT DNA Library Preparation Kit	Illumina	Cat# FC-131-1024
Chromium Single Cell 5′ Library & Gel Bead Kit	10*x* Genomics	Cat# 1000006

(*Continued on next page*)

Please cite this article in press as: Hashimoto et al., CD4 CTLs in supercentenarians: Signs of adaptive expansion in healthy aging, Cell Reports (2026), https://doi.org/10.1016/j.celrep.2026.117728

Continued

REAGENT or RESOURCE	SOURCE	IDENTIFIER
Chromium Single Cell 5′ Feature Barcode Library Kit	10*x* Genomics	Cat# 1000080
Chromium Single Cell V(D)J Enrichment Kit, Human T cell	10*x* Genomics	Cat# 1000005
Deposited data		
Raw sequencing data	This paper	NBDC: hum0511; GEA: E-GEAD-1107 and E-GEAD-1108
Processed single-cell RNA-seq data	This paper	OUKA: https://hdl.handle.net/11094/104062
Pretrained VAE model and source code	This paper	OUKA: https://hdl.handle.net/11094/104062
Processed single-cell RNA-seq data	Yazar et al.[28]	https://cellxgene.cziscience.com/collections/dde06e0f-ab3b-46be-96a2-a8082383c4a1
Processed single-cell RNA-seq data	Gong et al.[27]	https://apps.allenimmunology.org/aifi/resources/imm-health-atlas/downloads/scrna/
Processed single-cell RNA-seq data	Wang et al.[26]	https://www.synapse.org/Synapse:syn61609846
Processed single-cell RNA-seq data	Hashimoto et al.[10]	http://gerg.gsc.riken.jp/SC2018/
Processed single-cell RNA-seq data	Terekhova et al.[25]	https://www.synapse.org/Synapse:syn50542388
Processed single-cell RNA-seq data	Luo et al.[24]	https://www.ncbi.nlm.nih.gov/geo/query/acc.cgi?acc=GSE157007
Software and algorithms		
Cell Ranger v6.1.2	10*x* Genomics	https://www.10xgenomics.com/support/software/cell-ranger/downloads
Seurat v4.1.1	Hao et al.[30]	https://satijalab.org/seurat/
R v4.1.3	The R Project	https://www.r-project.org/
freebayes v1.3.5	Garrison et al.[55]	https://github.com/freebayes/freebayes/releases
vcftools v0.1.16	Danecek et al.[56]	https://vcftools.github.io/
demuxlet	Kang et al.[57]	https://github.com/statgen/demuxlet
STAR	Dobin et al.[58]	https://github.com/alexdobin/STAR
CellTypist	Dominguez Conde et al.[29]	https://www.celltypist.org/
TensorFlow	Google Brain	https://www.tensorflow.org/

EXPERIMENTAL MODEL AND STUDY PARTICIPANT DETAILS

The use of human blood samples in this study was approved by the Keio University School of Medicine Ethics Committee (Approval No. 2002-1020-27), The University of Osaka Research Ethics Committee (Approval No. 939), and RIKEN Ethical Review Committee (Approval No. H28-6). This study included 28 Japanese donors: eight donors aged 70s–90s, ten centenarians, and ten supercentenarians. Age and sex information for each donor is summarized in Figure S1A.

METHOD DETAILS

Isolation of T cells from human blood samples

Blood samples were collected in 2-mL EDTA tubes after obtaining informed consent from each donor. T cells were extracted from whole blood using SepMate-15 tubes (STEMCELL Technologies), RosetteSep Human T cell Enrichment Cocktail (STEMCELL Technologies), and Ficoll-Paque Plus in accordance with the manufacturer's guidelines. The RosetteSep cocktail was added to the blood and incubated for 10 min to enrich T cells via negative selection. Diluted blood (1:1 with phosphate-buffered saline and 2% FBS) was then placed in SepMate tubes and centrifuged at 1200 × *g* for 10 min at room temperature. The resultant mononuclear cells underwent washing with the same buffer, followed by double centrifugation at 300 × *g* for 8 min. A Countess II Automated Cell Counter

(Thermo Fisher Scientific) was employed for assessing cell count and viability. CELLBANKER 2 (1 mL) was added per 0.5 to 1 million cells, and aliquots were cryopreserved at −80°C.

Labeling of cell surface proteins

Cryopreserved T cells were thawed in a 37°C water bath for 2 min. After the exterior of the vial was sanitized with 70% ethanol, the cells were transferred to a 2-mL tube. The cryovial was rinsed with 1 mL of 10% FBS medium. After centrifugation at 500 × g for 5 min, the supernatant volume was reduced to 200 μL. Cells were resuspended with incremental additions of medium. Chromium Single Cell 5′ Feature Barcode Library Kit and TotalSeq-C (BioLegend) were used for pooling multiple samples with specific hashtags and profiling 16 selected surface proteins. The conjugates of antibodies and oligonucleotides containing a feature barcode were mixed in a 1.5-mL tube and centrifuged at 14,000 × *g* for 10 min at room temperature. For cell labeling, 0.2 to 1 million cells were centrifuged, and the pellet was resuspended in 50 μL labeling buffer, treated with Human TruStain FcX and dextran sulfate, and incubated for 10 min at 4°C. Following a 60-min incubation with the antibody mix, cells were washed and centrifuged. The final cell pellet was resuspended in 1.0 mL resuspension buffer.

Preparation of single-cell transcriptome, cell surface protein, and TCR libraries

Chromium Single Cell 5′ Library & Gel Bead Kit and V(D)J Enrichment Kit (Human T cell) were used to prepare the single-cell libraries following manufacturer's protocols. Two to three samples were pooled before loading into the 10*x* Chromium Controller, in which each cell was encapsulated in a droplet with unique barcoded oligonucleotides, enzymes, and other reagents. In each cell, RNAs were reverse transcribed into cDNAs incorporating unique cell and molecular barcodes. The barcoded cDNAs were amplified via PCR for the transcriptome library. VDJ segments were enriched with primers specific to the TCR constant regions for the TCR library. TCRα and TCRβ chains were obtained as paired sequences from the same cell using the 10*x* Genomics V(D)J protocol. DNAs containing feature barcode oligonucleotides were used to construct the cell surface protein library. The libraries were sequenced on the MGI-Seq2000 platform.

Processing of the primary single-cell sequence data

The sequencing data were processed using Cell Ranger version 6.1.2. The FASTQ files from three types of libraries (transcriptome, cell surface protein, and TCR) were processed together using *cellranger multi* with refdata-gex-GRCh38-2020-A as a reference genome and refdata-cellranger-vdj-GRCh38-alts-ensembl-5.0.0 as a reference VDJ sequence. The results of *cellranger multi* from each experiment were aggregated into a single output using *cellranger aggr* with default parameters. The original source of each cell was identified based on the UMI counts of sample-specific hashtags (Figures S1B–S1D). Low-quality cells were excluded based on four criteria (Figures S1E and S1F). First, cells without a single type of hashtag were excluded because of their uncertain sample assignment (indicated in green in Figures S1C and S1D). Second, cells with CD3 feature barcode UMI counts <100 were excluded, as they were classified as non-T cells (Figure S1G). Third, cells with mitochondrial gene expression >10% were removed (indicated in green in Figure S1F). Finally, cells with feature barcode UMI counts exceeding 10,000 were considered to be antibody aggregation and thus removed (indicated in red in Figure S1F). The UMI count matrix was loaded into the Seurat R package (version 4.1.1)[30] in R (version 4.1.3). Integration of transcriptome and surface protein profiles was conducted using the FindMultiModalNeighbors function, employing the first 30 principal components for the transcriptome and 15 for surface proteins. Cell clustering and dimensional reduction (UMAP) were performed using the FindClusters and RunUMAP functions, respectively. Clonal diversity was quantified using the Simpson's index: $\lambda = \frac{\sum n_i(n_i-1)}{N(N-1)}$ and the Shannon diversity index: $H' = -\sum \frac{n_i}{N} \ln\left(\frac{n_i}{N}\right)$, where n_i is the number of cells in clone i and N is the total number of cells.

PMA and ionomycin stimulation for secondary single-cell analysis

Cryopreserved T cells were thawed in a 37°C water bath for 2 min. The vial was sanitized with 70% ethanol. After the cells were transferred, the cryovial was rinsed with 1 mL of 10% FBS medium. The cells were then centrifuged at 500 × *g* for 5 min, resuspended, and transferred to a 96-well plate at 100–200 μL per well. Stimulation was performed using a cell activation cocktail containing phorbol 12-myristate 13-acetate (PMA) and ionomycin (BioLegend), along with brefeldin A (eBioscience). After 6 h of incubation, Hashtag1 and Hashtag3 (TotalSeq-C, BioLegend) were used to label the stimulated and unstimulated cells, respectively, after which both populations were pooled for single-cell library preparation. Transcriptome, surface protein, and TCR libraries were then prepared using the Chromium Single Cell 5′ Library & Gel Bead Kit and V(D)J Enrichment Kit (Human T cell) (10*x* Genomics), following the protocol previously described. The libraries were sequenced on the MGI-Seq2000 platform.

Processing of the secondary single-cell sequence data

The sequencing data were processed using Cell Ranger version 6.1.2, with the same parameters and reference files as described for the primary data. Low-quality cells were excluded based on the same four criteria used for the primary data, with the additional exclusion of cells lacking detectable TCR sequences. The UMI count matrix was loaded into the Seurat R package (version 4.1.1) in R (version 4.1.3), with integration, clustering, and UMAP reduction performed as described for the primary data.

In this experiment, because all samples were pooled before sequencing, individual cells were assigned to donors based on SNPs. SNP calling was performed on the primary single-cell sequencing data using freebayes v1.3.5,[55] excluding the Y chromosome. Filtering was conducted with vcftools v0.1.16,[56] applying minimum mean depth 10, minimum quality value 30, and restricted to exonic SNPs defined by GENCODE v36.[59] Using the resulting set of 18,813 SNPs and the aligned bam files, each cell was assigned to a donor using demuxlet.[57] Cells that could not be uniquely assigned to a single donor were excluded from the analysis. Stimulated and unstimulated conditions were determined based on the counts of Hashtag1 and Hashtag3.

Flow cytometry, cell sorting, and bulk RNA-seq

Peripheral blood mononuclear cells from two donors were stained with antibodies against CD3, CD4, CD45RO, CD27, and CD28, together with 7-AAD for viability assessment, and analyzed by flow cytometry. After gating on live $CD3^{+}CD4^{+}$ T cells, the $CD27^{-}CD28^{-}$ subset and the CD45RO + $CD28^{+}$ subset were identified and sorted directly into MagMAX lysis buffer. Total RNA was isolated using the MagMAX mirVana Total RNA Isolation Kit. Full-length cDNA was then synthesized and amplified using the SMART-Seq mRNA workflow with LD-PCR amplification. Sequencing libraries were prepared from amplified cDNA using the Nextera XT DNA Library Preparation Kit and sequenced on a NovaSeq X platform. After adapter trimming and quality control, reads were aligned to the reference genome using STAR,[58] and gene expression levels were summarized as counts per million (CPM).

Prediction of CD4 CTLs in public datasets

To identify CD4 CTLs from transcriptome data alone, a multi-task Variational Autoencoder (VAE) was developed in TensorFlow. The model was designed to receive RNA expression profiles as input and simultaneously perform RNA reconstruction, surface protein (ADT) prediction, and cell-type classification (Figure S1M). The encoder received log-transformed RNA expression profiles that were aligned with a standardized reference list of 6,585 genes used in CellTypist.[29] These profiles were concatenated with sample identities, represented as one-hot vectors, to regress out technical batch variations. The input was compressed into a 16-dimensional latent space using a dropout rate of 0.2. To prevent overfitting to cell-type labels and to learn generalized latent representations, the decoder comprised three distinct branches corresponding to these tasks. The joint loss function was defined as the weighted sum of the mean squared errors for RNA and ADT reconstructions, the sparse categorical cross-entropy for cell-type classification, and the Kullback-Leibler (KL) divergence for latent space regularization. The model was trained on the primary dataset of 28 samples. One sample from each group (A01, B01, and C01) was assigned to the validation set, while the remaining 25 samples were used for training. Optimization was performed using the AdamW optimizer with a learning rate of 1e−3 and a batch size of 256 for 30 epochs.

To test the generalizability of the trained VAE model on independent external data, we utilized a published PBMC reference atlas dataset (10*x* Genomics 3′ single-cell, GSE164378).[30] In this dataset of 161,764 cells, immune cells including CD4 CTLs had been previously defined using a panel of 228 surface antibodies (ADTs). Relying solely on RNA input, we evaluated the predictive performance (precision, recall, and F1-score) against these cell-type labels across 10 runs with different random seeds.

Following model construction, training, and external testing, the VAE was applied to evaluate age-associated changes in CD4 CTLs across large-scale populations. Single-cell RNA-seq datasets of peripheral blood mononuclear cells (PBMCs) and isolated T cells were collected from six public cohorts and combined with the present study (Figure S1K). Raw UMI count matrices from the public datasets were processed similarly. Cell-type labels were subsequently inferred for all cells using the trained VAE model, relying solely on the RNA modality, and the fraction of predicted CD4 CTLs per sample was calculated.

QUANTIFICATION AND STATISTICAL ANALYSIS

All statistical analyses were performed using R (version 4.1.3). Monotonic trends across age groups were assessed using the two-sided Jonckheere–Terpstra test (jonckheere.test function). The Wilcoxon rank-sum test (wilcox.test function) was used for two-group comparisons. For comparisons among three or more groups, the Kruskal–Wallis test (kruskal.test function) was used, followed by Dunn's post hoc test (dunnTest function from the FSA package) with Bonferroni correction. To evaluate differences in subtype composition across major CD4 CTL clones, a chi-squared test with simulated *p*-value (chisq.test function with simulate.p.value = TRUE and B = 100,000) was applied to a clone-by-subtype contingency table. Asterisks denote significance levels: $*p < 0.05$, $**p < 0.01$, $***p < 0.001$.